GEOPHYSICS, VOL. 79, NO. 5 (SEPTEMBER-OCTOBER 2014); P. D349–D362, 17 FIGS., 5 TABLES.
10.1190/GEO2014-0023.1

Measurements of elastic constants in anisotropic media

Bradley C. Abell[1], Siyi Shao[1], and Laura J. Pyrak-Nolte[2]

ABSTRACT

Simulation of elastic-wave propagation in rock requires knowledge of the elastic constants of the medium. The number of elastic constants required to describe a rock depends on the symmetry class. For example, isotropic symmetry requires only two elastic constants, whereas transversely isotropic symmetry requires five unique elastic constants. The off-diagonal elastic constant depends on a wave velocity measured along a nonsymmetry axis. The most difficult barrier when measuring these elastic constants is the ambiguity between the phase and group velocity in experimental measurements. Several methods to eliminate this difficulty have been previously proposed, but they typically require several samples, difficult machining, or complicated computational analysis. Another approach is to use the surface (Rayleigh) wave velocity to obtain the off-diagonal elastic constant. Rayleigh waves propagated along symmetry axes have phase and group velocities that are equal for materials with no frequency dispersion, thereby eliminating the ambiguity. Using a theoretical secular equation that relates the Rayleigh velocity to the elastic constants enable determination of the off-diagonal elastic constant. Laboratory measurements of the elastic constants in isotropic and anisotropic materials were made using ultrasonic transducers (central frequency of 1 MHz) for the Rayleigh-wave method and a wavefront-imaging method. The two methods indicated agreement within 1% and 3% for isotropic and transversely isotropic samples, respectively, demonstrating the ability of the Rayleigh-wave method to measure the off-diagonal elastic constant. The surface-wave approach eliminates the need for multiple samples, expensive computational calculations, and most importantly, it removes the ambiguity between the phase and group velocity in the measured data for materials with no frequency dispersion because all measurements are made along symmetry axes.

INTRODUCTION

Anisotropy was originally studied for applications to light propagation in an elastic ether by Lord Kelvin and others, and the work was later expanded to more diverse fields such as geophysics (Helbig, 1994; Schoenberg and Sayers, 1995; for a review, Helbig and Thomsen, 2005), metals (Aussel and Monchalin, 1989; Kohlhauser and Hellmich, 2012), crystals (Wang, 1995; Wolfe, 1998; Jakata and Every, 2008), wood (Bucur and Archer, 1984; Najafi et al., 2005), and even industrial applications such as musical instruments and brake pads (Bucur, 2006; Sanders and Yuhas, 2007). Measuring the elastic constants of a material evolved from static methods to resonance methods, ultrasound laser methods, and more commonly, wave transmission methods (Aussel and Monchalin, 1989; Jakata and Every, 2008). Several nice reviews of these methods can be found in the references (Every, 1994; Wolfe, 1998).

The wave-transmission method was applied to materials using a wide range of frequencies, but it traditionally required many measurements and many samples to be prepared. For example, Bucur and Archer (1984) measured the elastic constants of several wood species by preparing samples that were cut at 0°, 15°, 30°, and 45° to the symmetry axis. Christensen and Ramanantoandro (1971) performed a similar measurement on dunite but used samples cut from 0° to 90° in 15° increments. These samples, although from the same type of material, might have exhibited internal differences in structure, composition, symmetry, or densities. These differences between samples might lead to spurious values for the measured elastic constants and may result in artifacts in the analysis of the main sample under consideration. A more ideal approach would measure all of the elastic constants on the same sample.

Manuscript received by the Editor 17 January 2014; revised manuscript received 8 May 2014; published online 19 August 2014.
[1]Purdue University, Department of Physics and Astronomy, West Lafayette, Indiana, USA. E-mail: babell@purdue.edu; shao5@purdue.edu.
[2]Purdue University, Department of Physics and Astronomy, School of Civil Engineering, and Department of Earth, Atmospheric, and Planetary Sciences, West Lafayette, Indiana, USA. E-mail: ljpn@purdue.edu.

The general symmetry classes of anisotropic elastic media are well defined and can be found in any introductory book on anisotropy (e.g., Bucur and Archer, 1984; Mavko et al., 1998). Each symmetry class is defined based upon the number of terms that are unique to the elastic stiffness tensor. For isotropic media, there are two unique elastic constants, commonly referred to as the Lamé parameters. For vertically transversely isotropic (VTI) media, there are five unique elastic constants, and for orthotropic media, there are nine. These constants can be written in a matrix notation (see the "Results and Analysis" section) and are symmetric about the diagonal. The difficulty in measuring all of the elastic constants in the same sample arises from the need to obtain the off-diagonal terms.

For isotropic samples, the P- and S-wave velocities are the same in all directions (e.g., $C_{11} = C_{22} = C_{33}$, $C_{44} = C_{55} = C_{66}$), leading to spherical wavefronts propagating through the material. For anisotropic materials, the velocities are no longer the same in every direction, giving rise to nonspherical wavefronts (Wolfe, 1998). The phase and group angles are no longer equal because the wavefronts are not spherical in shape. The angle between the normal to the wavefront and the unique axis is the phase angle, θ; the angle between the normal to the source plane and the direct line from the source to the receiver location is the group angle, ϕ (see Figure 1)

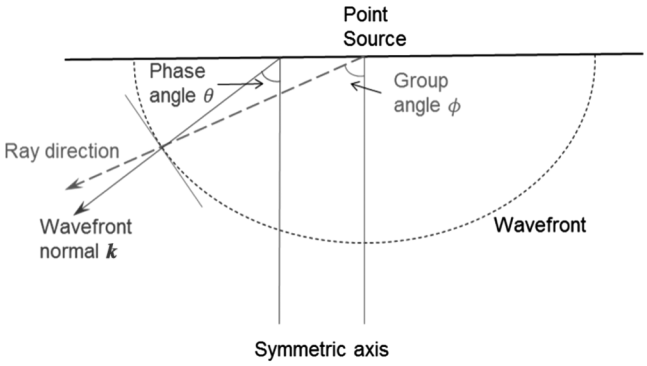

Figure 1. Pictorial representation of the difference between the phase and group angles for a nonspherical wavefront. The wavefront (dashed line) originates from a point source, typically outside of the sample surface (solid line), and spreads throughout the sample. At the measurement location, the phase angle, θ, is defined as the angle made with the normal to the wavefront (**k**) and the plane of the point source. The group angle, ϕ, is defined by the angle made with the straight (ray) path from the source to the receiver, as shown.

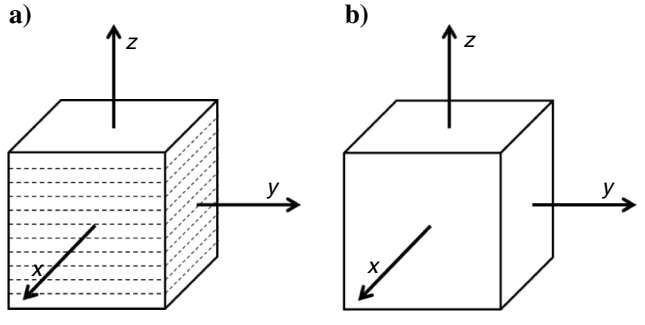

Figure 2. (a) Phenolic G10 sample and (b) acrylic sample geometry. The dashed lines, which are not drawn to scale, represent the layering.

(Thomsen, 1986). For VTI media, P-wave velocities are the same in two orthogonal directions and are different in the third. The direction in which the wave velocities differ from the other two orthogonal axes is the unique axis (e.g., the z-axis in Figure 2a). The shape of the wavefront must be known to determine the phase angle θ in nonorthogonal directions to the symmetry axes. The phase angle is then used to calculate the phase velocity (Thomsen, 1986), and thus not knowing the shape of the wavefront can lead to a misinterpretation of the phase angle, phase velocity, and, therefore, the elastic constants.

The group angle ϕ of the wavefront surface is used to determine the group velocity. The relationship between the group and phase velocities (or angles) is difficult to calculate without taking measurements at several angles, due to the derivative of the phase velocity with respect to phase angle (see equation 4) (Berryman, 1979; Thomsen, 1986; Tsvankin, 1996, 1997). In addition, difficulty arises in determining which velocity (group or phase) is actually measured with the type of transducer used (Every and Sachse, 1990; Dellinger and Vernik, 1994; Vestrum, 1994; Wolfe, 1998). A rule of thumb set forth by Dellinger and Vernik (1994) is that the ratio of the propagation path length to transducer illumination width needs to be $\geq$20 to measure the group velocity, and $\leq$3 to measure the phase velocity. If the ratio falls between or near these values, great care must be taken to determine which value is actually measured.

Numerical techniques have also been developed to calculate the off-diagonal elastic constants using these velocity measurements. Although these approaches were typically very robust and intensive (i.e., large computational programs were required to extract the elastic constants), they required more information than was available for cube-shaped samples (Castagnede et al., 1990; Wang, 1995). To determine all 21 independent elastic constants, 21 measurements, along different directions, must be made for each sample. This leads to difficulty in determining how to cut the sample(s). The best option would be to cut the sample into a sphere and make the required measurements. However, this approach requires complicated machining, and the measurement of shear waves through spheres can be difficult to obtain depending on the sample size and wavelengths used (Helbig, 1994). In this paper, we demonstrate that the off-diagonal elastic constants can be determined from measurements on cubic samples that do not require complicated sample preparation.

Recently, surface and interface waves have been used to determine elastic constants. Dahmen et al. (2010) used air-coupled transducers and the velocity of Lamb waves to determine the elastic constants of anisotropic media. Others (Deresiewicz and Mindlin, 1957; Bucur and Rocaboy, 1988) used the bicubic equation for surface acoustic waves to invert and obtain the elastic constants. The drawbacks to this technique are that it requires three types of transducers, two for bulk wave measurements (S and P) and one for surface acoustic waves, and it requires a sample cut at 45° to the symmetry axis. Shao and Pyrak-Nolte (2013) used the results from the interface wave to determine the C_{13} parameter, but the approach was not explicitly verified. Work has also been done to develop transducers that transmit waves at oblique angles to a surface, avoiding the need for a specialized cut; this approach again requires the use of three types of transducers (Sharf-Aldin et al., 2013).

This paper describes a method to determine the off-diagonal elastic constants (e.g., C_{13}) for media with no frequency dispersion using the Rayleigh-wave velocity. Abell and Pyrak-Nolte (2013)

recently use this technique to determine C_{13} in an aluminum sample, but they did not verified or explicitly explained the technique. Although the Rayleigh wave was predicted more than 125 years ago by Lord Rayleigh (1885), explicit solutions for the isotropic Rayleigh velocity as a function of the bulk velocities, as opposed to the secular equation, were only recently derived (Rahman and Barber, 1995; Mechkour, 2002). This solution was later analyzed by several authors to develop an even simpler approximate expression for the velocity in isotropic and anisotropic media using various mathematical techniques (Vinh and Ogden, 2004b; Li, 2006; Rahman and Michelitsch, 2006; Nkemzi, 2008).

Among the explicit solutions derived for the Rayleigh-wave velocity, Vinh and Ogden (2004a) obtained a simple expression for the Rayleigh velocity in orthotropic media as a function of the elastic constants (see equation 3.28 in Vinh and Ogden, 2004a). The expression is easily extended from orthotropic to higher symmetries following the formulation of Chadwick (1976). This expression, discussed in the "Analysis" section of this paper, allows the C_{13} (or C_{12}) value to be easily calculated from the Rayleigh velocity and bulk waves that travel through the sample.

The Rayleigh-wave method has the advantage of only requiring two contact transducers (shear [S] and compressional [P]), one sample aligned with the symmetry axes, and one simple equation to solve for the elastic constants. In this study, the method was applied to an isotropic acrylic sample to verify that the technique works on isotropic media, and to an anisotropic sample. To verify the measured results, a wavefront-imaging (WFI) method was performed on the same samples to obtain a value of C_{13} using the anisotropic techniques first put forth by Thomsen (1986). In this paper, it is demonstrated that the two techniques are equivalent but that the Rayleigh technique has many experimental and theoretical benefits.

EXPERIMENTAL APPROACH

Sample description

A WFI method and a Rayleigh velocity method were used to determine the elastic constants of both an isotropic and an anisotropic sample. The isotropic sample was an acrylic (Lucite) cube with smooth, milled surfaces. The anisotropic sample was phenolic G10, an epoxy glass laminate with layer spacing on the order of 500 μm, that was also machined to obtain smooth surfaces. See Table 1 for the dimensions and physical parameters of the two materials and Figure 2 for the alignment of the samples with the coordinate system.

Phenolic G10 was chosen for the anisotropic sample because of its high-quality synthetic layering (i.e., good transverse anisotropy) without significant background effects from heterogeneous distributions of small-scale minerals typically found in rocks.

Acoustic wavefront imaging method

In the acoustic WFI experiment, two spherically focused water-coupled piezoelectric transducers (Panametrics V303-SU) with a central frequency of 1 MHz, a nominal element size of approximately 13 mm, and a focal point of 2 mm were used. As stated in the "Introduction" section, the ratio of the sample height to the transducer illumination size is important in determining which velocity is being measured. For the isotropic and anisotropic samples, this ratio was 50.8 and 50.9, respectively, indicating that the velocities measured were well within the group velocity regime (i.e., ≥20 based on the rule of thumb set forth by Dellinger and Vernik, 1994).

The source transducer was located at a fixed position, and the receiver transducer was scanned over a 2D region to capture the arriving wavefront. The receiver position was controlled by two computer-controlled (Newport ESP300) linear actuators (Newport Model 850B). A pulse generator (Panametrics model 5077PR) sent an excitation pulse (400 V square pulse) to the source transducer. The pulse width was 0.3 μs with a repetition rate of 100 Hz. Received signals were collected through a 14-bit digitizer (National Instruments USB-5133) and stored on a computer.

For testing, a sealed sample was placed in a water tank (Figure 3) and held with a nominal load (≤0.5 kN) to ensure that the sample did not move during scanning. The sample was sealed using 3M 3765 clear label protection tape applied to each face of the sample with all of the air bubbles removed. The corners of the sample were sealed using Coghlan's 8880 Airstop, a commercial liquid sealant. The sample was submerged because water-coupled transducers were used to ensure uniform coupling between the transducers and the sample for all measured positions. The surfaces of the source, the sample, and the scanning plane of the receiver were aligned

Table 1. Sample dimensions for the directions shown in Figure 2. All sizes have an uncertainty of ±0.03 mm, and the density has an uncertainty of ±1.0 kg/m^3.

Direction	Isotropic acrylic	Anisotropic phenolic G10
x (m)	0.09975	0.10170
y (m)	0.10150	0.10170
z (m)	0.09982	0.10170
Density (kg/m^3)	1184.0	1936.6

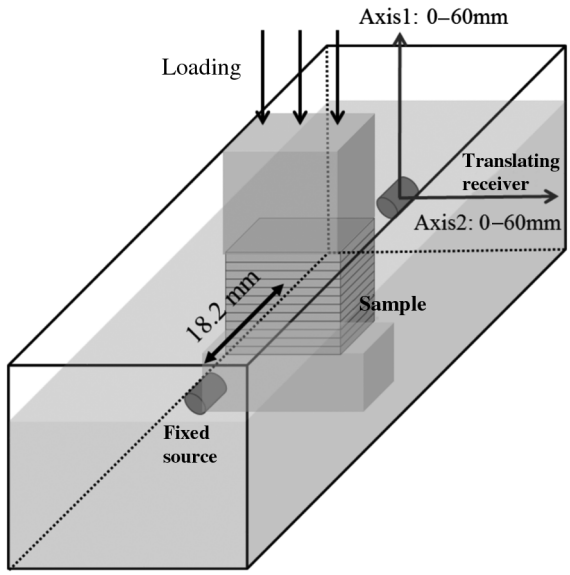

Figure 3. Experimental setup for the WFI experiment. Note that the sample and transducers are submerged in water and only the receiver transducer translates.

parallel by minimizing the reflection times from the surface of a sample. The distance between the source/receiver and the sample surface was set to the focal length of the transducer (~18.2 mm) to ensure that the transducer was focused on the surface. The receiver was translated in 1 mm increments to scan the sample from the center line (when the source and receiver were aligned) to a distance 50–60 mm away from the center line (Figure 4). For these distances, the maximum group angle with respect to the symmetry axis was 30° (ϕ in Figure 4) for the sample sizes used in this study.

Figure 5 shows the shift in arrival time of the P-wave signals for the acrylic sample (Figure 5a) and the G10 sample (Figure 5b) when the receiver was translated away from the source (i.e., center line). As the distance between the source and receiver increased (as well as the wave travel path), the transmitted signals arrived later. An S-wave is also required to calculate the elastic constants in the WFI technique. The same S-wave used to calculate C_{44} in the Rayleigh-wave technique was used in the WFI analysis below.

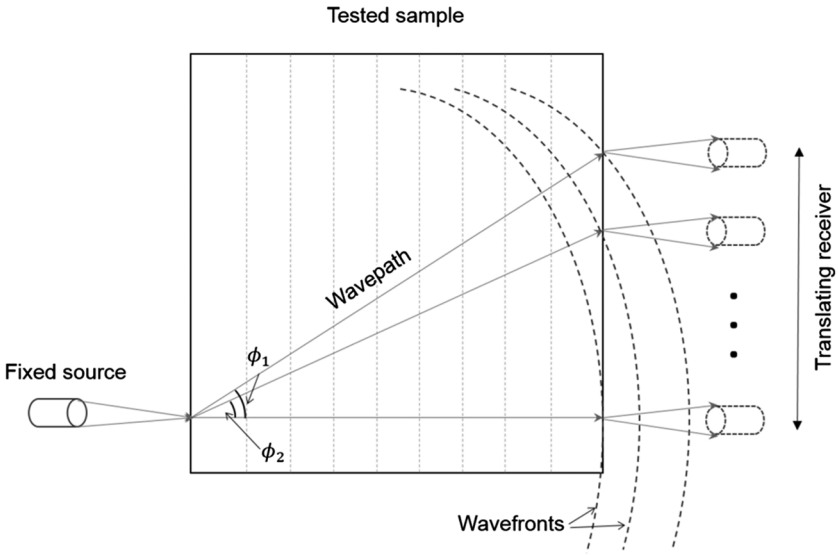

Figure 4. WFI experimental setup for the phenolic G10 sample. Note that the source transducer is fixed (left) and the receiver transducer (right) translates to measure the wavefront over the entire surface of the sample. The vertical dashed lines represent the orientation of the layering in the phenolic G10, and the curved dashed lines represent the wavefront.

Rayleigh-wave method

For the Rayleigh-wave technique, P- and S-waves were sent and received using piezoelectric contact transducers (Olympus-Panametrics V103 and V153) that have a central frequency of 1 MHz and an element size of 13 mm. Honey, with 8.75% (by weight) of the water removed through convection heating at 90°C for ~120 minutes, was used as a couplant between the sample and transducer. A square-wave pulse of 400 V, with a 1 kHz repetition rate from an Olympus 5077PR pulse generator, was used to excite the source transducers. The received signals were recorded using a 14-bit digitizer 100 MSamples/s oscilloscope (National Instruments USB-5133) and stored on a computer for later analysis.

Only four measurements (Figure 6) are necessary to determine the off-diagonal elastic stiffness value (C_{13}); however, for thoroughness, measurements of the P-, S-, and Rayleigh waves

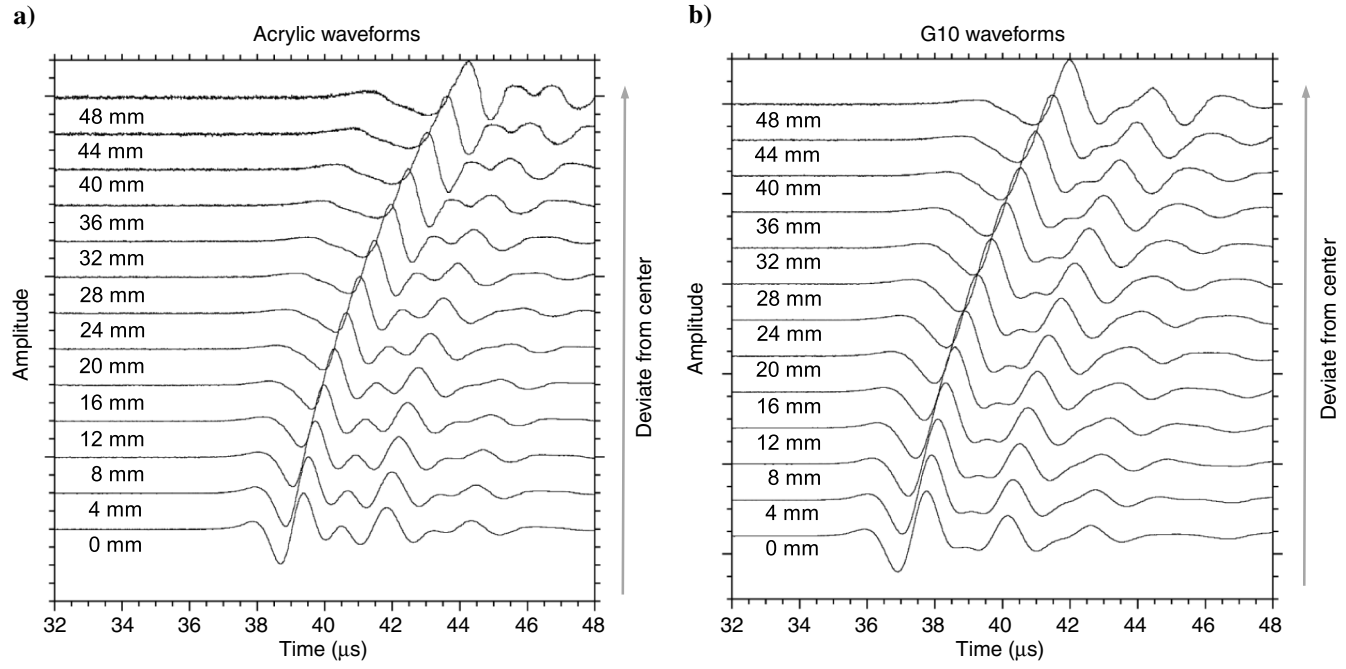

Figure 5. The received signals from the WFI tests for: (a) the acrylic sample and (b) the phenolic G10 sample (propagated through the layers) when the receiver was deviated from the aligned position with the source. Note that the source and receiver were aligned at 0 mm.

for each direction and in each polarization were measured for the isotropic and anisotropic samples (see Tables 1–3 and Figures 7 and 8).

For the acrylic sample, the P- and S-waves were determined to be the same in all directions (Figure 7, Table 2) as expected for an isotropic sample. For the G10 phenolic sample, the P- and S-waves were the same along the x- and y-directions (which are parallel to the layering), but differed along the z-direction (which is perpendicular to the layering), indicating a VTI sample (Figure 8). However, the S-wave propagating in the x-direction (see Figure 2 for directions) acquired some energy from the y polarization, indicating that the transducer was not purely polarized (middle S-wave of Figure 8). This was also observed for waves propagating in the y-direction and polarized in the x-direction.

A Morlet wavelet analysis was performed, only on the first arrival, to calculate the group velocity (Pyrak-Nolte and Nolte, 1995; Nolte et al., 2000). The group velocities were obtained for a frequency of 0.5 MHz and are listed in Tables 2 and 3. In the Rayleigh-wave method, the phase and group velocities were equivalent because all measurements were taken along symmetry axes.

RESULTS AND ANALYSIS

Wavefront imaging

In the acoustic WFI experiment, the group angle ϕ was equal to zero at the central point of the wavefront when the receiver transducer was aligned with the source transducer (Figure 4). When the receiver was translated horizontally N mm away from the center, the transmitted signal corresponded to a nonzero group angle $\phi = \tan^{-1}(N/l)$, where l is the length of the sample, in millimeters (see Table 1).

From these measurements, the elastic stiffness constants C_{ij} were calculated using two relationships: the relationship between the group and phase angle and the relationship between the group and phase velocity (equation 4). VTI media (Figure 2a) have five independent elastic stiffness components ($C_{11}, C_{33}, C_{44}, C_{66}$, and C_{13}) in contrast to an isotropic medium (Figure 2b) that has only two independent elastic components (one corresponding to the body P-wave (C_{11}) and the other corresponding to the body S-wave (C_{66}) (Helbig, 1994; Bucur, 2006). The elastic stiffness tensor of a VTI medium, with its unique axis aligned with the z-direction, can be written in matrix form as

$$\mathbf{C} = \begin{pmatrix} C_{11} & C_{11}-2C_{66} & C_{13} & 0 & 0 & 0 \\ C_{11}-2C_{66} & C_{11} & C_{13} & 0 & 0 & 0 \\ C_{13} & C_{13} & C_{33} & 0 & 0 & 0 \\ 0 & 0 & 0 & C_{44} & 0 & 0 \\ 0 & 0 & 0 & 0 & C_{44} & 0 \\ 0 & 0 & 0 & 0 & 0 & C_{66} \end{pmatrix}. \quad (1)$$

The elastic stiffness tensor relates stress to strain

$$\sigma_{ij} = C_{ijkl}\epsilon_{kl}, \quad (2)$$

where σ are the stresses and ϵ are the strains and summations are suppressed (Mavko et al., 1998). For the subscripts in equations 1 and 2, the Voigt notation (e.g., $1232 = 64$) has been applied to simplify the tensor notation into a 6×6 matrix. The subscripts

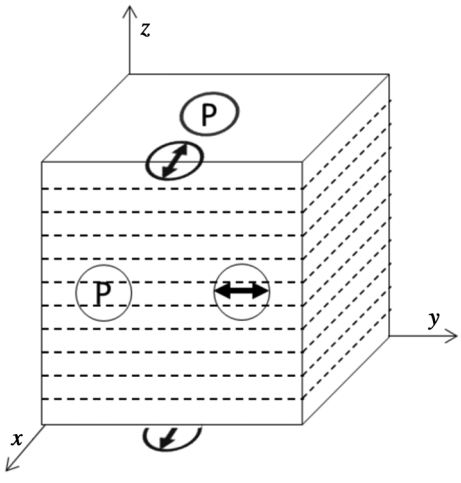

Figure 6. Rayleigh-wave method experimental setup. The circles with arrows indicate the orientation of the S-wave transducers, and the circles with P indicate the orientation of the P-wave transducers for measurements made on the phenolic G10 sample.

Table 2. Measured isotropic acrylic and anisotropic phenolic G10 wavelet velocities, for a frequency of 0.5 MHz. The first parenthesis is the propagation direction, the second is the polarization, and the third is the unit.

Parameter	Isotropic acrylic	Anisotropic phenolic G10
P-wave velocity (x) (any) (m/s)	2646.7 ± 0.8	3571.5 ± 0.8
P-wave velocity (y) (any) (m/s)	2651.9 ± 1.0	3617.6 ± 0.8
P-wave velocity (z) (any) (m/s)	2651.2 ± 0.8	2850.0 ± 0.8
S-wave velocity (x) (y) (m/s)	1358.4 ± 0.5	1713.8 ± 1.0
S-wave velocity (x) (z) (m/s)	1358.9 ± 0.5	1491.0 ± 0.4
S-wave velocity (y) (x) (m/s)	1362.6 ± 0.5	1705.4 ± 0.9
S-wave velocity (y) (z) (m/s)	1362.8 ± 0.5	1496.6 ± 0.4
S-wave velocity (z) (x) (m/s)	1362.1 ± 0.5	1481.5 ± 0.4
S-wave velocity (z) (y) (m/s)	1361.7 ± 0.5	1493.9 ± 0.4

Table 3. Measured isotropic acrylic and anisotropic phenolic G10 Rayleigh velocities. The first parenthesis is the propagation direction, the second is the polarization, and the third is the unit. All listed uncertainties are one standard deviation from the measurements made in each direction at different positions on the sample.

Parameter	Isotropic acrylic	Anisotropic phenolic G10
Rayleigh-wave wavelet velocity (z) (x) (m/s)	1257.6 ± 1.0	1435.0 ± 0.8
Rayleigh-wave wavelet velocity (z) (y) (m/s)	1263.6 ± 1.0	1435.0 ± 0.8

represent the propagation and polarization directions, where $i = 1, 2, 3$ represents the x-, y-, and z-directions, respectively.

In equation 1, C_{11}, C_{33}, C_{44}, and C_{66} are the diagonal components, which can be obtained directly by measuring body-wave velocities along the coordinate axes and the density of the VTI sample (Bucur, 2006). The terms C_{11} and C_{33} depend on the density and P-wave velocity, whereas C_{44} and C_{66} depend on the density and S-wave velocity. The off-diagonal term C_{13} is affected by the wave

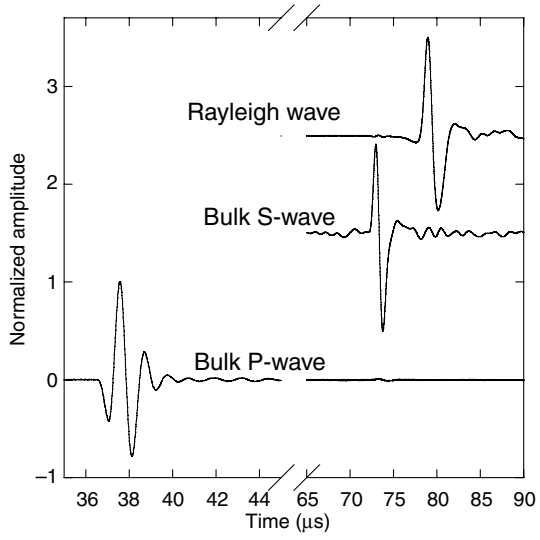

Figure 7. Signals transmitted through the acrylic sample from the Rayleigh technique. The bulk P-, bulk S-, and Rayleigh waves are all shown for reference. Measurements from all orthogonal directions yielded the same arrival times, within the uncertainties listed in Tables 2 and 3. Note that the amplitudes have been normalized.

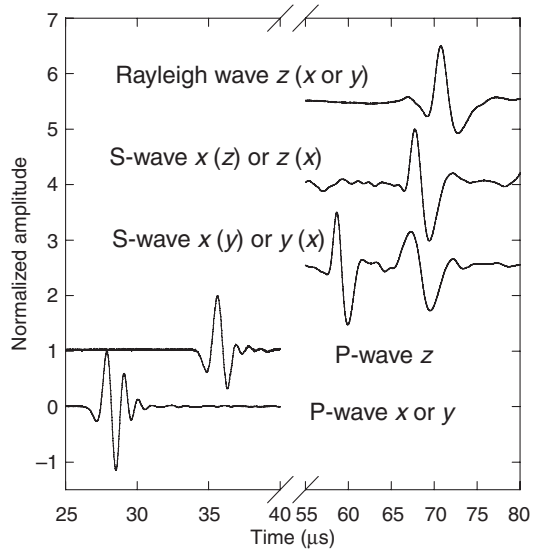

Figure 8. Signals transmitted through the phenolic G10 sample from the Rayleigh technique. The bulk P-, bulk S-, and Rayleigh waves are shown for reference. The first letter represents the propagation direction from the axes shown in Figure 2. The direction in the parenthesis represents the polarization of the S-wave transducer. Note that the amplitudes have been normalized.

velocities of P- and S-waves, propagating at an angle other than 0° or 90° with respect to the symmetry axis. Equation 3 gives the form of the directionally dependent phase velocity as a function of phase angle θ, in a VTI medium with no frequency dispersion and was used to obtain C_{13} (Thomsen, 1986):

$$\begin{aligned}
\rho v_{\mathrm{P}}^2(\theta) &= \frac{1}{2}[C_{33} + C_{44} + (C_{11} - C_{33})\sin^2\theta + D(\theta)];\\
\rho v_{\mathrm{SV}}^2(\theta) &= \frac{1}{2}[C_{33} + C_{44} + (C_{11} - C_{33})\sin^2\theta - D(\theta)];\\
\rho v_{\mathrm{SH}}^2(\theta) &= C_{66}\sin^2\theta + C_{44}\cos^2\theta;\\
D(\theta) &= \sqrt{[(C_{33} - C_{44})\cos^2\theta - (C_{11} - C_{44})\sin^2\theta]^2 + (C_{13} + C_{44})^2\sin^2(2\theta)};
\end{aligned} \tag{3}$$

where ρ is the material density and θ is the phase angle. The terms v_{SV} and v_{SH} refer to the S-wave phase velocity propagating with a component in the unique direction (z-axis in Figure 2a) and with no component in the unique direction, respectively. The off-diagonal P- and SV-wave velocities (v_{P} and v_{SV}) depend on C_{13} through the $D(\theta)$ term.

It is important to again clarify the distinction between the phase angle, θ, and the group angle, ϕ. The phase angle is measured between the symmetry axis and the wavefront-normal direction $\mathbf{k}$, whereas the group angle indicates the ray angle from the source to the wavefront receiver location (Figure 1) (Thomsen, 1986; Helbig, 1994). In isotropic media (Figure 2b), where the wavefronts are spherical, the group angle is always equal to the phase angle (i.e., $\phi = \theta$); in anisotropic media (Figure 2a), where the wavefronts are distorted or may be ellipsoidal in shape, the group angle does not equal the phase angle, except along symmetry directions.

The relationships between the phase angle, θ, and group angle, ϕ, in a VTI medium, as well as that between the phase velocity, v, and group velocity, V', were derived by Thomsen (1986) as

$$\begin{aligned}
\tan(\phi) &= \frac{(v\ \sin\theta + \frac{dv}{d\theta}\ \cos\theta)}{(v\ \cos\theta - \frac{dv}{d\theta}\ \sin\theta)},\\
V'(\phi) &= \sqrt{v^2(\theta) + \left(\frac{dv}{d\theta}\right)^2}.
\end{aligned} \tag{4}$$

The difference between the phase and group angles are difficult to separate in experimental measurements of the off-diagonal elastic components (C_{13} in this case). Acoustic WFI techniques provide a noninvasive way to address this issue. Using a combination of focused, water-coupled ultrasonic transducers and precise motion steppers, the signals for waves propagated along different travel paths through a VTI medium can be obtained (see Figures 3 and 4).

To calculate C_{13} in a VTI medium using a WFI method, the following steps are required: (1) a transformation between the phase angle, θ, and group angle, ϕ, using the value of C_{13} assumed in equation 3; (2) using equation 3 to calculate the phase velocity, v, corresponding to a specific phase angle, θ; (3) calculating the theoretical group velocity, V', using equation 4; and then (4) comparing it to the experimentally measured group velocity, V, for verification.

Geometrically, group angles can be obtained as ϕ_1 and ϕ_2, shown in Figure 4, and the traveltimes through different paths in the sample can be obtained from a first-break analysis, or by applying a Morlet wavelet-analysis (Pyrak-Nolte and Nolte, 1995; Nolte et al.,

2000) to the transmitted signals. Using the peak from the wavelet as the traveltime, instead of the signal's first-break point, when using focused water-coupled transducers is verified in the following section for the isotropic sample. As long as the distance between the source focal point and the receiver focal point is known, group velocities that correspond to a certain group angle can be calculated.

The WFI technique generates a data set from which experimental group velocities as a function of group angles can be extracted. A least-squares fit procedure was applied to compare the squared sum of the difference between the experimental and theoretical group velocities that were obtained by changing the C_{13} values (Figure 9) in equations 1–4. The experimentally measured C_{13} value of the VTI sample corresponds to the "best-fit" C_{13}, which matches the least-squares fit procedure.

Wavefronts from the acrylic sample and the phenolic G10 sample using the WFI method are shown in Figure 10. The acrylic sample is isotropic (i.e., no preferred direction), and the wavefront is observed to be circular in shape (Figure 10a). Wavefronts were also recorded for two orientations of the phenolic G10 sample relative to the source: (1) wave propagation parallel to the layers (Figure 10b) and (2) wave propagation normal to the layers (Figure 10c). The phenolic G10 sample is a tight laminate with a unique direction (normal to the layering), which is expected for a VTI media. The wavefronts in Figure 10b from the phenolic G10 sample are elliptical because the P-wave propagates faster parallel to the layers than perpendicular to the layers. The wavefronts in Figure 10c are nearly circular, similar to an isotropic sample, because the waves propagated along the sample's unique axis and had nearly identical velocities in the two directions parallel to the layering.

In this study, group time delays were obtained through a wavelet transformation of the ultrasonic signals from the experimental measurements (Pyrak-Nolte and Nolte, 1995; Nolte et al., 2000). Using a wavelet transformation, the group arrival time of the maximum amplitude at the dominant frequency was determined. The group arrival time was then used to calculate the group velocity. For a transmitted signal, the group time delay is always different from the first-break/onset delay (Möllhoff et al., 2010). *First break* indicates the first recorded transmitted signal attributed to the energy generated by the source, and *group delay* refers to the delay of the wave packet. In WFI, it was hypothesized that the group delay better represented the travel path than the first-break delay for a trans-

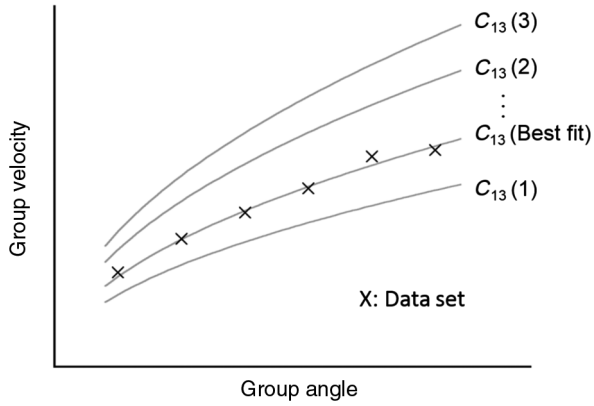

Figure 9. Best fit of C_{13} to a theoretical curve based on the WFI analysis. The solid lines represent theoretical curves, using different C_{13} values, and the x symbols represent a possible data set. This example shows our fitting approach. The sample data set is to demonstrate the concept and does not correspond to the measured data in this paper.

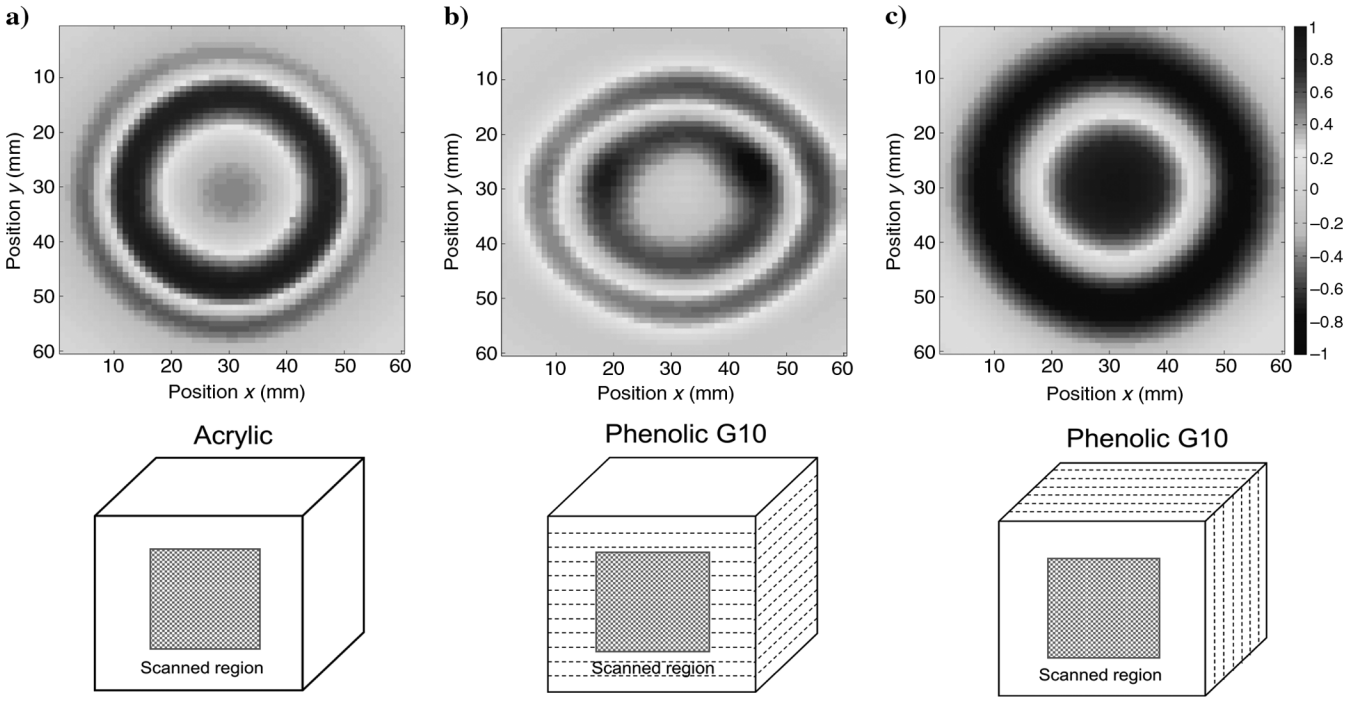

Figure 10. Two-dimensional snapshots (60 × 60 mm) of arriving wavefronts for (a) the acrylic sample, (b) the phenolic G10 sample when waves were propagated parallel to the layering, and (c) the phenolic G10 sample when waves were propagated perpendicular to the layering. The colors in the 2D snapshots represent the normalized amplitude of the signals: Dark colors correspond to high amplitude, and vice versa.

mitted acoustic signal from the focal point of the source transducer to the focal point of the receiver transducer. These group delays were compared to the first-break delays and to the theoretical requirements for group velocities to determine which method gave the true group velocity.

For the acrylic sample, the first-break velocities were measured by picking the onset time of the received signal (Figure 5a). Because the acrylic sample is essentially isotropic (Table 2), the first-break velocity should, theoretically, be independent of the group angle. However, the first-break velocity was found to increase as the group angle increased (circles in Figure 11). The contradiction between the experimental results and theoretical prediction indicated that picking the first-break points of the transmitted signals was not suitable to compute correctly the wave velocities. Figure 11 also shows that the wavelet velocities (squares in Figure 11), obtained from Morlet wavelet analysis, were independent of angle. Thus, the wavelet velocity was used as the group velocity for the acoustic WFI experiment.

The diagonal elastic constant components were calculated using equation 3 (and the elastic constants listed in Table 4) and were used to generate a curve to best fit the experimental data (solid line in Figure 11). Using this technique, the value of the off-diagonal term, C_{13}, in the acrylic sample was measured to be $4.03 \pm 0.05 (\pm 1.2\%)$ GPa.

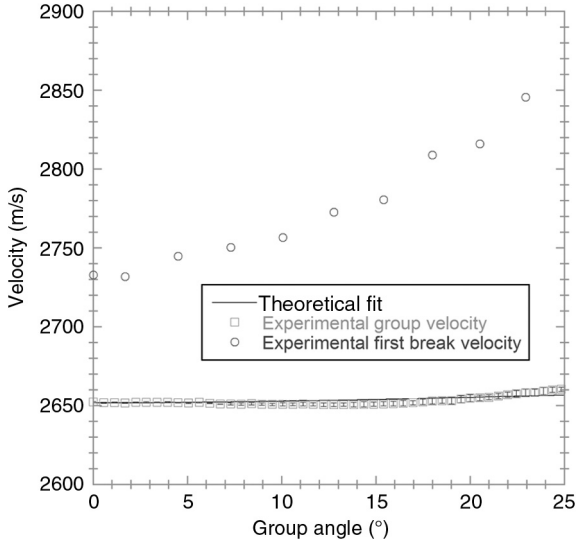

Figure 11. Theoretical best fit to C_{13} for data from the acrylic sample. Also shown are the first-break velocity and group velocity as a function of group angle.

Table 4. Elastic constants calculated from the wavelet values in Tables 1 and 2. The units are listed in the parenthesis. Errors were calculated using standard error techniques (see Appendix A).

Parameter	Isotropic acrylic	Anisotropic phenolic G10
C_{11} (GPa)	8.294 ± 0.009	24.703 ± 0.016
C_{33} (GPa)	8.322 ± 0.009	15.730 ± 0.0012
C_{55} (GPa)	2.186 ± 0.002	4.305 ± 0.003

The group velocity, V, in the phenolic G10 cube depends on the group angle, ϕ. In a VTI medium, with no frequency dispersion, when the group angle, ϕ, equals zero, the P-wave propagates perpendicularly to the layers, which corresponds to the lowest wave speed. However, when the receiver deviates from the center (Figures 4 and 5), the group velocity increases as ϕ increases (Figure 12). This again verified that the wavelet analysis correctly measured the group velocity.

The procedure used to compute C_{13} in the acrylic sample was then applied to the data from the phenolic G10 cube. The calculated value of C_{13} in the phenolic G10 sample, using this method, was $8.0 \pm 0.3 (3.8\%)$ GPa.

Rayleigh-wave method

Equation 2 must be combined with the equation of motion for a continuum to calculate the elastic constants from the Rayleigh-wave method. The relationship between the elastic constants, C_{ijkl}, and phase velocity, v, for waves propagated in a particular direction are summarized by the Christoffel equations (Bucur, 2006):

$$\Gamma_{ik} = C_{ijkl} n_j n_l, \tag{5}$$

and

$$(\Gamma_{ik} - \delta_{ik} \rho v^2) P_m = 0, \tag{6}$$

where Γ represents the Christoffel tensor, ρ is the density, n_i are the direction cosines, δ_{ik} is the Kronecker delta function, P_m is the component of the unit vector in the displacement direction, and C_{ijkl} are the elastic constants. For a full derivation, see Bucur (2006).

These relationships can be written out, explicitly, for each term in the elastic stiffness tensor (C_{ijkl}) to determine their values based on the phase velocity of the waves propagated in a particular direction. For the C_{13} term, the full expression is

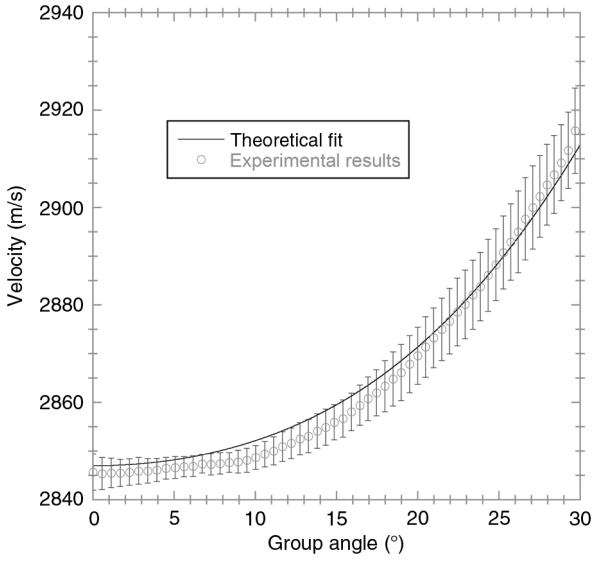

Figure 12. A comparison of the best-fit theoretical group velocity as a function of group angle and the experimentally measured group velocity. Error bars show the range of values from repeated measurements.

$$v_{13} = \sqrt{\frac{1}{2\rho}\left\{(\Gamma_{11} + \Gamma_{33}) + \sqrt{[(\Gamma_{11} - \Gamma_{33})^2 + 4\Gamma_{13}^2]}\right\}}, \tag{7}$$

and for a 45° propagation direction with respect to the symmetric axis, equation 7 can be expanded as

$$v_{13} = \sqrt{\frac{1}{\rho}\left\{\frac{C_{55}}{2} + \frac{C_{33} + C_{11}}{4} + \frac{\sqrt{[(C_{33} - C_{11})^2 + 4(C_{13} + C_{55})^2]}}{4}\right\}}, \tag{8}$$

where v_{13} is the P-wave velocity propagated at 45° with respect to the $x - z$-plane (quasi-P). Equation 8 can be easily manipulated to obtain C_{13} as a function of the phase velocity. The difficulty, as discussed in the "Introduction," is in obtaining the correct phase velocity at a known phase angle (e.g., 45° here).

To avoid the ambiguity in determining the correct cophasal surface, this paper presents a method to determine the off-diagonal stiffness value from the Rayleigh velocity measured on a sample with no frequency dispersion. The benefits of using a Rayleigh wave are as follows: only one sample is required, the same S-wave transducer used on the bulk can be used to measure the surface wave, and the propagation direction is aligned with one of the symmetry axes (and thus the phase and group velocities are equal) removing any uncertainty as to which velocity is measured. The relationship between the elastic constants of an orthotropic medium and the Rayleigh-wave velocity has been recently obtained by Vinh and Ogden (2004a). The Rayleigh velocity, V_{ray}, in an orthotropic medium is expressed as

$$V_{\text{ray}} = \sqrt{\frac{C_{55}\sqrt{\alpha}\sigma\Delta}{\rho}\left[\sqrt{\alpha}\frac{(\sigma\Delta + 2)}{3} + \sqrt[3]{R + \sqrt{D}} + \sqrt[3]{R - \sqrt{D}}\right]^{-1}}, \tag{9}$$

where

$$\begin{aligned}
&\alpha = \frac{C_{33}}{C_{11}}, \quad \Delta = 1 - \frac{C_{13}^2}{C_{11}C_{33}}, \quad \sigma = \frac{C_{11}}{C_{55}}, \\
&a_0 = -\sqrt{\alpha}(1 - \Delta), \quad a_2 = \sqrt{\alpha}(1 - \sigma\Delta), \\
&R = -\frac{1}{54}(2a_2^3 + 9a_2 + 27a_0), \\
&D = R^2 + \left[-\left(\frac{1}{3}\sqrt{a_2^2 + 3}\right)^2\right]^3,
\end{aligned} \tag{10}$$

where C_{ij} are the elastic constants (written in Voigt notation) and ρ is the density. Recall that only four measurements must be made: two P-waves along symmetry axes, one S-wave, and the Rayleigh wave. From these four measurements, C_{11}, C_{33}, C_{55} and a value of C_{13} can be easily determined from equations 6, 9, and 10.

The expression for the Rayleigh velocity (equation 9) was obtained for general orthotropic (orthorhombic) symmetry and agrees with the previously derived secular equation for the Rayleigh velocity found by Chadwick (1976). Vinh and Ogden (2004a) also verified that this result reverts to the isotropic equation when the correct material parameters are used, indicating the usefulness of equation 9 for any symmetry classes from isotropic to orthotropic.

An important transformation for other material symmetries was briefly mentioned by Vinh and Ogden (2004a), but the importance needs to be further emphasized here. For symmetries in the transversely isotropic domain, a substitution of variables depends on the orientation of the symmetry axes (Chadwick, 1976). When the material possesses higher symmetry than orthotropic, e.g., VTI, the symmetry of the problem increases allowing pure surface modes to exist in all directions. Along the symmetry directions, these surface modes should be identical and can be verified using the positive definiteness of the strain energy (for a full description, see Chadwick, 1976).

The measured Rayleigh- and bulk-wave velocities, for the isotropic and anisotropic samples, were used to calculate values of C_{11}, C_{33}, and C_{55} (see Table 4) using the aforementioned Rayleigh velocity method. These values were then applied to equation 9 to obtain the theoretical curves that relate C_{13} to the Rayleigh velocity (Figures 13 and 14). From these theoretical curves, the values of the Rayleigh velocity, measured on both samples (see Table 3), were used to estimate the value of C_{13}.

For the isotropic case, the value of $C_{13}(C_{12})$ was found to be in good agreement with the theoretical value for C_{13} in isotropic media, which can be derived from the following relation (Helbig, 1994; Mavko et al., 1998; Bucur, 2006):

$$C_{13} = C_{11} - 2C_{55}. \tag{11}$$

Using equation 11, the theoretical value for the isotropic acrylic sample is $C_{13}^{\text{theory}} = 3.92 \pm 0.01(\pm 0.25\%)$ GPa. This value is in agreement with the estimated value from the Rayleigh velocity method, using the curve in Figure 13 ($C_{13} = 4.06 \pm 0.19(\pm 4.6\%)$ GPa), and the WFI method ($4.03 \pm 0.05(\pm 1.2\%)$ GPa) as shown in Table 5. The difference between the two experimental methods was 0.03 ± 0.20 GPa, indicating a good agreement between the C_{13} values obtained by the two techniques; thus verifying the applicability of the Rayleigh velocity method for isotropic media.

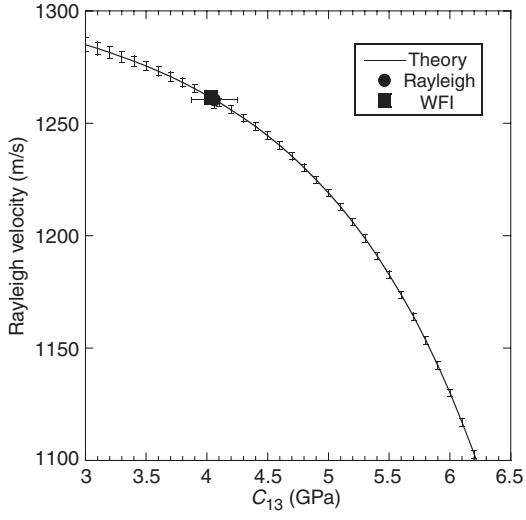

Figure 13. Rayleigh velocity as a function of C_{13}, from equation 9, using the acrylic parameters in Tables 1–3. The error bars in the theory were calculated using the elastic constant error bars in Table 4 (see Appendix A). The Rayleigh wave and WFI C_{13} results are shown and indicate agreement.

In the anisotropic phenolic G10 sample, the Rayleigh-wave technique (Figure 14) yields a value of $C_{13} = 7.7 \pm 0.7 (\pm 9\%)$ GPa. The value obtained using the WFI method is 8.0 ± 0.3 ($\pm 3.8\%$) GPa. The absolute difference between these two values is 0.3 ± 0.8 GPa, again indicating a good agreement. These results are summarized in Table 5.

DISCUSSION

Wavefront imaging

Two experimental methods were used to determine C_{13} for an isotropic and anisotropic medium with no frequency dispersion. Both methods are based on measuring group velocities but differ in the complexity of the experiments and analysis. However, the WFI method and the Rayleigh-wave method yielded similar values of C_{13} to within 0.3 ± 0.8 GPa for an anisotropic medium.

The WFI approach uses the relationship between the phase and group angles, as well as the phase and group velocity in a transversely isotropic media, to determine the off-diagonal elastic component. From the experimental results presented here for the acrylic and phenolic G10 samples, the WFI technique produced smaller uncertainties when compared with the Rayleigh-wave method, and it was highly repeatable. Some advantages of using this method include: the ability to image surfaces that are not smooth and having a full view of the wavefront surface throughout the sample.

There are major disadvantages to using the WFI method, including the measurement time, theoretical analysis, and sealing of the sample. Typical measurements are >0.5 hours, whereas the Rayleigh-wave method requires <1 minute. Analysis of the WFI method requires careful consideration of the subtle differences in group and phase angles, as discussed above. In addition, the WFI method only applies for symmetries up to VTI symmetry, whereas the theory for the Rayleigh-wave method exists up to orthorhombic symmetry. The sample must be waterproofed (i.e., sealed) to be submerged in water, and the size of the sample must be small enough to fit in the experimental setup, but not so small that reflections from the edges are measured. All of these disadvantages are circumvented using the Rayleigh-wave method.

Table 5. The C_{13} values, fit from the theoretical curves in Figures 12 and 13, using the Rayleigh-wave technique, and measured using the WFI technique. The difference indicates that these two measurements are in agreement, where a value of 0 indicates perfect agreement.

Parameter	Isotropic acrylic	Anisotropic phenolic G10
C_{13} (GPa) Rayleigh method	4.06 ± 0.19	7.7 ± 0.7
C_{13} (GPa) WFI method	4.03 ± 0.05	8.0 ± 0.3
Absolute difference |Rayleigh – WFI|	0.03 ± 0.20	0.3 ± 0.8

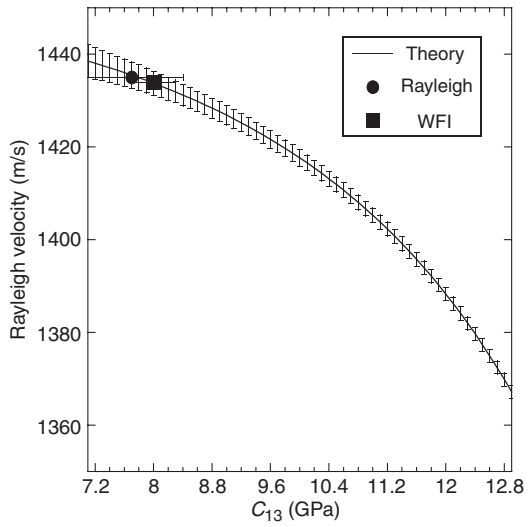

Figure 14. Rayleigh velocity as a function of C_{13} from equation 9 using the phenolic G10 parameters in Tables 1–3. The error bars in the theory were calculated using the elastic constant error bars in Table 4 (see Appendix A). The Rayleigh-wave and WFI C_{13} results are shown.

Uncertainty in the Rayleigh-wave method

For the Rayleigh-wave method, the experimental uncertainties arose from the sample size, point-to-point variations, traveltime, and calculated velocity from the wavelet; therefore, uncertainties in the diagonal elastic constants were all from inherent experimental uncertainties in the setup and design.

The sample size is within the machining tolerances usually expected for samples (i.e., 25 μm tolerances). The measurement time was limited by the sampling rate of the USB 5133 NI digitizer. The sampling rate for this experiment was set to 100 MSteps/s for 10,000 steps. This leaves each bin with a sampling size of 0.01 μs. The obtained waveforms were analyzed using Morlet wavelets with 8192 increments over the 10,000 steps. This left the calculated wavelet time step at 0.012 μs/step, which is twice the time uncertainty in the experiment.

Applying these uncertainties in time and distance yields an uncertainty in velocity, purely from experimental limitations, on the order of ±0.8 m/s for P-waves and ±0.4 m/s for S- and Rayleigh waves in the isotropic and anisotropic samples measured in this study. These uncertainties are small (i.e., ~0.1%) and are of the same order as the standard deviation from repeated measurements at the same position. The larger of the two values is listed in Tables 2 and 3.

These velocity uncertainties were used to calculate the uncertainties in the elastic constants (Appendix A and Table 4), which were again small (i.e., ~0.03%). The uncertainties were then used to calculate an uncertainty in the estimated Rayleigh velocity from equation 9 (see Appendix A). Normal error propagation techniques were used to calculate these uncertainties (Taylor, 1997). The results are shown as the error bars in the Rayleigh velocity plots in Figures 13 and 14.

Applications to rock

Material parameters from the literature were analyzed to determine if the Rayleigh-wave method would apply to rock. Elastic constants from the literature (Musgrave, 1970; Thomsen, 1986; Christensen, 1989; Martinez and Schmitt, 2013) were used in the Rayleigh-wave method (equations 6–10) to determine a possible

Rayleigh-wave velocity based on the measured elastic constants. Theoretical curves using these material properties are shown for three common materials (shale, dolomite, and sandstone) in Figure 15. The circles in Figure 15 represent the experimentally measured values for these three samples from the literature. For all three samples, the theoretical curves reach an asymptote at low C_{13} values. If the measured Rayleigh velocity falls within 1% of the asymptotic value, the estimated C_{13} has an uncertainty too great to have any physical significance. If the measured value is below 1% of this asymptotic line, then the uncertainty in the measurement is acceptable, and the method can be applied.

To determine whether the Rayleigh-wave method could be applied to the materials in the literature, the Rayleigh-wave velocity was normalized by the maximum, such that a percentage of the maximum theoretical Rayleigh-wave velocity could be determined as a function of C_{13} for the materials under study. The results are shown in Figure 16 for different types of rock and natural materials.

The resulting Rayleigh-wave velocities from the literature analysis (Figure 16) indicate that for some samples this technique would apply well (points below the dashed line in Figure 16) and for others it would not (points above the dashed line in Figure 16). In order for this technique to apply, the Rayleigh-wave velocity percentage of the max must be below 0.99 in Figure 16, such that if the Rayleigh velocity were measured with 1% uncertainty, the value of C_{13} from the theory would fall below the asymptotic values, as shown in Figure 15, for low C_{13} values.

The materials listed by Thomsen (1986) were given as a function of pressure and were used to explore the relationship between the theoretical Rayleigh-wave velocity percentage and applied pressure. The results are shown in Figure 17, and they demonstrate that an increase in pressure resulted in an increase in the Rayleigh-wave velocity percentage, indicating that the samples may have contained microcracks or other stress-sensitive structures. The data indicated that as the pressure was increased, the velocities changed such that the Rayleigh velocity, based upon the measured S-wave velocity and elastic constants, increased with the pressure (Figure 17). Thus, at high pressures, the Rayleigh-wave technique would yield C_{13} values with large uncertainties. In addition, the presence of microcracks and fractures can result in frequency dispersion that would cause the group and phase velocity to differ even along the symmetry axes. Additional research is needed to examine the role of crack-induced frequency dispersion on the laboratory Rayleigh-wave method.

Laboratory measurements of the Rayleigh wave and bulk waves can be performed under pressure on cubic or core samples, but to the authors' best knowledge, this has not be done for this technique. For core samples, the length of the core needs to be sufficiently long to have a measurable difference in arrival time between the Rayleigh wave and the bulk S-wave. A rule of thumb, for a core length, l, based on the period, T, is

$$l \geq (TF)\left(\frac{V_{\text{shear}} V_{\text{Rayleigh}}}{V_{\text{shear}} - V_{\text{Rayleigh}}}\right), \tag{12}$$

where F is a factor of separation between the wave packet of the Rayleigh wave and bulk S-wave, V_{Rayleigh} is the Rayleigh velocity and V_{shear} is the S-wave velocity. As an example, $F = 1$ means that the wave packets are completely separated, $F = 0$ means that the wave packets occur simultaneously in time, and are indistinguishable, and $F = 0.5$ means that the Rayleigh wave begins exactly halfway through the wave packet of the bulk S-wave.

Although the two wave speeds only need to be separated by a small amount (e.g., 1%), it is best if the two wave packets are at least separated by 50%, resulting in a value of $F = 0.5$ for the core. For the isotropic sample velocities, at a frequency of 0.5 MHz, the resulting core length from equation 12 would be $l \geq 0.017$ m. The sample used was 0.099 m; the wave packets were well separated. Similarly for the phenolic G10 sample (along the z-direction), using a value of $F = 0.5$, equation 12 would yield a core length of

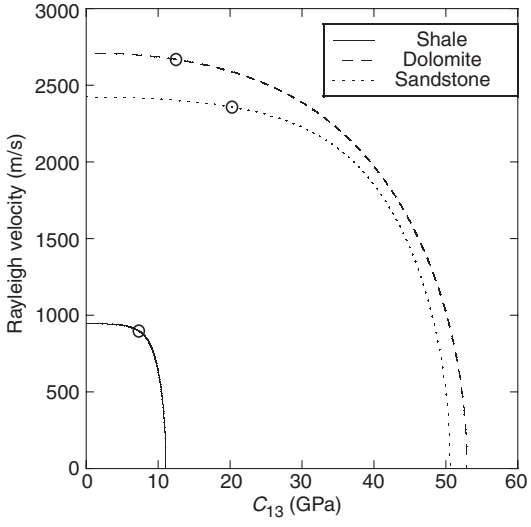

Figure 15. Comparison of the predicted Rayleigh-wave velocities for three rocks from the literature to theoretical curves of the Rayleigh velocity as a function of C_{13}. The circles represent the theoretical value of the Rayleigh velocity for the measured values of C_{13} from Thomsen (1986) and Martinez and Schmitt (2013).

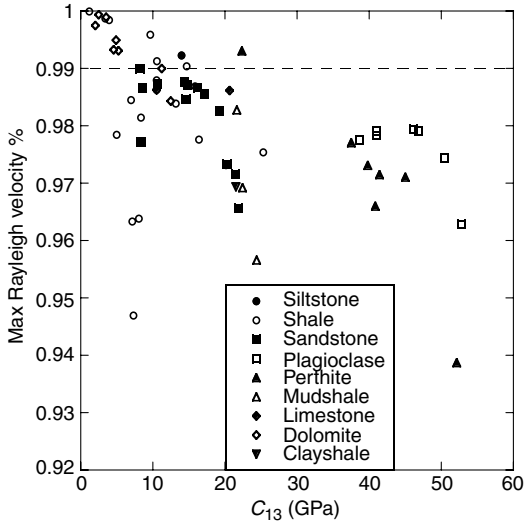

Figure 16. Theoretical Rayleigh velocity, as a percentage of the maximum theoretical Rayleigh velocity, shown as a function of the measured C_{13} for rocks from the literature (Musgrave, 1970; Thomsen, 1986; Christensen, 1989; Martinez and Schmitt, 2013). The dashed line represents the value above which this method would yield large uncertainties.

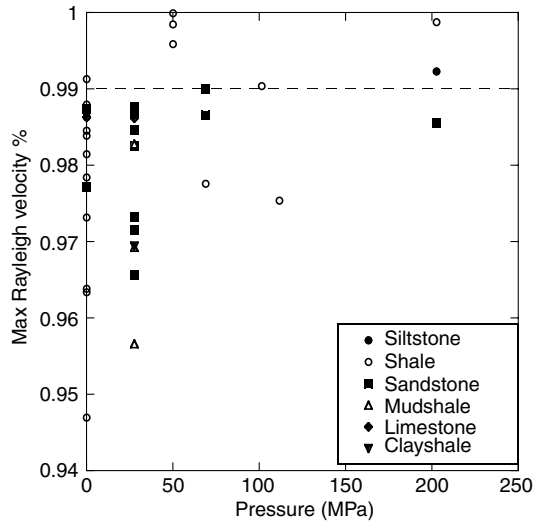

Figure 17. Theoretical Rayleigh velocity, as a percentage of the maximum theoretical Rayleigh velocity, shown as a function of the applied pressure. The data in this figure are from Thomsen (1986).

$l \geq 0.046$ m, again much smaller than the sample size used here (0.101 m).

CONCLUSIONS

The elastic constants of rock are often needed to simulate and understand wave propagation data from the Earth's subsurface and to obtain other rock properties of interest. The number of elastic constants required depends on the degree of symmetry in a rock. The Rayleigh-wave method for determining the off-diagonal elastic constant was demonstrated on laboratory samples with VTI. Estimates of C_{13} from measurements made with the Rayleigh method were within the uncertainties of C_{13} determined from the more time and computationally intensive WFI method. The benefits of using the Rayleigh-wave technique for determining the off-diagonal elastic constants of a VTI medium are (1) only one sample is needed, (2) only two contact transducers (P- and S-) are required, (3) the analysis technique does not require complicated calculations of wavefronts or angles, (4) only four measurements are required (three bulk waves and one surface wave, all along symmetry axes) to obtain an estimate of C_{13}, and (5) the method can be applied to symmetries from isotropic to orthotropic media. Although cubic samples were used in this study, the Rayleigh-wave technique can be adapted for use on cylindrical cores. The technique can easily be performed on samples under uniaxial, biaxial, and true triaxial loading conditions. However, additional theoretical and experimental research is needed to adapt the Rayleigh-wave technique for testing in pressure vessels and to determine the effect of frequency dispersion from cracks on the interpretation.

ACKNOWLEDGMENTS

The authors wish to acknowledge support of this work by the Geosciences Research Program, Office of Basic Energy Sciences United States Department of Energy (DE-FG02-09ER16022), and the Geo-Mathematical Imaging Group (GMIG) at Purdue University.

APPENDIX A

UNCERTAINTY CALCULATION

This appendix discusses the calculation of uncertainty in the experimental Rayleigh-wave method measurements. When two values (x and y), each with an uncertainty (δx and δy), are added or subtracted, the uncertainty of the result is calculated from (Taylor, 1997)

$$q = (x \pm \delta x) \pm (y \pm \delta y), \quad \delta q = \sqrt{(\delta x)^2 + (\delta y)^2}. \quad \text{(A-1)}$$

Similarly, the uncertainty of a product or quotient of these two values (x and y) is calculated from

$$q = (x \pm \delta x)(y \pm \delta y), \quad \text{or} \quad q = \frac{x \pm \delta x}{y \pm \delta y}$$
$$\delta q = |q| \sqrt{\left(\frac{\delta x}{x}\right)^2 + \left(\frac{\delta y}{y}\right)^2}, \quad \text{(A-2)}$$

and for values raised to the power n, the uncertainty is calculated by

$$q = (x \pm \delta x)^n \quad \delta q = |q||n| \frac{\delta x}{|x|}. \quad \text{(A-3)}$$

Using the identities in equations A-1, A-2, and A-3 applied to the measurements of the variables in equation 10, the uncertainty is calculated from

$$\delta\alpha = |\alpha| \sqrt{\left(\frac{\delta C_{33}}{C_{33}}\right)^2 + \left(\frac{\delta C_{11}}{C_{11}}\right)^2},$$
$$\delta\Delta = \left|\frac{C_{13}^2}{C_{11}C_{33}}\right| \sqrt{\left(\frac{\delta C_{33}}{C_{33}}\right)^2 + \left(\frac{\delta C_{11}}{C_{11}}\right)^2},$$
$$\delta\sigma = |\sigma| \sqrt{\left(\frac{\delta C_{55}}{C_{55}}\right)^2 + \left(\frac{\delta C_{11}}{C_{11}}\right)^2},$$
$$\delta a_0 = \sqrt{\left(\frac{1}{2}|\sqrt{\alpha}|\frac{\delta\alpha}{|\alpha|}\right)^2 + \left(|\sqrt{\alpha}\Delta| \sqrt{\left(\frac{\frac{1}{2}|\sqrt{\alpha}|\frac{\delta\alpha}{|\alpha|}}{\sqrt{\alpha}}\right)^2 + \left(\frac{\delta\Delta}{\Delta}\right)^2}\right)^2},$$
$$\delta a_2 = \sqrt{\left(\frac{1}{2}|\sqrt{\alpha}|\frac{\delta\alpha}{|\alpha|}\right)^2 + \left(|\sqrt{\alpha}\sigma\Delta| \sqrt{\left(\frac{\frac{1}{2}|\sqrt{\alpha}|\frac{\delta\alpha}{|\alpha|}}{\sqrt{\alpha}}\right)^2 + \left(\frac{\delta\sigma}{\sigma}\right)^2 + \left(\frac{\delta\Delta}{\Delta}\right)^2}\right)^2},$$
$$\delta R = \sqrt{\left(\frac{-6}{54}|a_2^3|\frac{\delta a_2}{|a_2|}\right)^2 + \left(\frac{-9}{54}\delta a_2\right)^2 + \left(\frac{-27}{54}\delta a_0\right)^2},$$
$$\delta D = \sqrt{2R^2\left(\frac{\delta R}{|R|}\right)^2 + \left(3\left|\left[\frac{-a_2^2}{9} - \frac{1}{3}\right]^3\right| \frac{\frac{2}{9}|a_2^2|\frac{\delta a_2}{|a_2|}}{\left|\frac{-a_2^2}{9} - \frac{1}{3}\right|}\right)^2}. \quad \text{(A-4)}$$

The above results were used to calculate the uncertainty in the Rayleigh velocity as

$$\delta V_{\text{Rayleigh}} = \frac{1}{2}|V_{\text{Rayleigh}}| \times \sqrt{\left(\frac{\delta\gamma}{\gamma}\right)^2 + \left(\frac{\sqrt{(\delta\Omega)^2 + (\delta\epsilon)^2 + (\delta\xi)^2}}{\left|\frac{\sqrt{\alpha}(\sigma\Delta+2)}{3} + \sqrt[3]{R+\sqrt{D}} + \sqrt[3]{R-\sqrt{D}}\right|}\right)^2}, \tag{A-5}$$

where

$$\frac{\delta\gamma}{\gamma} = \sqrt{\left(\frac{\delta C_{55}}{C_{55}}\right)^2 + \left(\frac{\delta\sigma}{\sigma}\right)^2 + \left(\frac{\delta\Delta}{\Delta}\right)^2 + \left(\frac{\delta\rho}{\rho}\right)^2 + \left(\frac{\delta\alpha}{2|\alpha|}\right)^2}, \tag{A-6}$$

$$\delta\Omega = \sqrt{\left[\left(\sqrt{\left(\frac{\delta\alpha}{2|\alpha|}\right)^2 + \left(\frac{\delta\sigma}{\sigma}\right)^2 + \left(\frac{\delta\Delta}{\Delta}\right)^2}\right)\left(\frac{\sqrt{\alpha}\sigma\Delta}{3}\right)\right]^2 + \left(\frac{\delta\alpha|\sqrt{\alpha}|}{3|\alpha|}\right)^2}, \tag{A-7}$$

$$\delta\epsilon = \frac{\left|\sqrt[3]{R+\sqrt{D}}\right|}{3}\frac{\sqrt{(\delta R)^2 + \left(\frac{|\sqrt{D}|}{2}\frac{\delta D}{|D|}\right)^2}}{|R+\sqrt{D}|}, \tag{A-8}$$

$$\delta\xi = \frac{\left|\sqrt[3]{R-\sqrt{D}}\right|}{3}\frac{\sqrt{(\delta R)^2 + \left(\frac{|\sqrt{D}|}{2}\frac{\delta D}{|D|}\right)^2}}{|R-\sqrt{D}|}. \tag{A-9}$$

The uncertainty in the Rayleigh velocity (equation A-5) is used to obtain the range of uncertainty in the estimated C_{13} value in this study.

REFERENCES

Abell, B., and L. J. Pyrak-Nolte, 2013, Coupled wedge waves: Journal of the Acoustical Society of America, **134**, 3551–3560, doi: 10.1121/1.4821987.

Aussel, J., and J. P. Monchalin, 1989, Precision laser-ultrasonic velocity measurement and elastic constant determination: Ultrasonics, **27**, 165–177, doi: 10.1016/0041-624X(89)90059-0.

Berryman, J., 1979, Long-wave elastic anisotropy in transversely isotropic media: Geophysics, **44**, 896–917, doi: 10.1190/1.1440984.

Bucur, V., 2006, Acoustics of wood: CRC Press, Inc.

Bucur, V., and R. Archer, 1984, Elastic constants for wood by an ultrasonic method: Wood Science Technology, **18**, 255–265, doi: 10.1007/BF00353361.

Bucur, V., and F. Rocaboy, 1988, Surface wave propagation in wood: Prospective method for the determination of wood off-diagonal terms of stiffness matrix: Ultrasonics, **26**, 344–347, doi: 10.1016/0041-624X(88)90033-9.

Castagnede, B., J. Jenkins, and W. Sachse, 1990, Optimal determination of the elastic constants of composite materials from ultrasonic wave-speed measurements: Journal of Applied Physics, **67**, 2753–2761, doi: 10.1063/1.345441.

Chadwick, P., 1976, The existence of pure surface modes in elastic materials with orthorhombic symmetry: Journal of Sound and Vibrations, **47**, 39–52, doi: 10.1016/0022-460X(76)90406-5.

Christensen, N., 1989, Seismic velocities, *in* R. Carmichael, CRC practical handbook of physical properties of rocks and minerals: CRC Press, Inc., 717.

Christensen, N., and R. Ramananantoandro, 1971, Elastic moduli and anisotropy of Dunite to 10 kilobars: Journal of Geophysical Research, **76**, 4003–4010, doi: 10.1029/JB076i017p04003.

Dahmen, S., H. Ketata, M. Ghozlen, and B. Hosten, 2010, Elastic constants measurement of anisotropic Olivier wood plates using air-coupled transducers generated Lamb wave and ultrasonic bulk wave: Ultrasonics, **50**, 502–507, doi: 10.1016/j.ultras.2009.10.014.

Dellinger, J., and L. Vernik, 1994, Do travel times in pulse transmission experiments yield anisotropic group or phase velocities?: Geophysics, **59**, 1774–1779, doi: 10.1190/1.1443564.

Deresiewicz, H., and R. Mindlin, 1957, Waves on the surface of a crystal: Journal of Applied Physics, **28**, 669–671, doi: 10.1063/1.1722827.

Every, A., 1994, Determination of the elastic constants of anisotropic solids: NDT & E International, **27**, 3–10, doi: 10.1016/0963-8695(94)90003-5.

Every, A., and W. Sachse, 1990, Determination of the elastic constants of anisotropic solids from acoustic-wave group-velocity measurements: Physical Review B: Condensed Matter and Materials Physics, **42**, 8196–8205, doi: 10.1103/PhysRevB.42.8196.

Helbig, K., 1994, Foundations of anisotropy for exploration seismics: Elsevier Science, Inc.

Helbig, K., and L. Thomsen, 2005, 75-plus years of anisotropy in exploration and reservoir seismics: A historical review of concepts and methods: Geophysics, **70**, no. 6, 9ND–23ND, doi: 10.1190/1.2122407.

Jakata, K., and A. Every, 2008, Determination of the dispersive elastic constants of the cubic crystals Ge, Si, GaAs, and InSb: Physical Review B, **77**, 174301, doi: 10.1103/PhysRevB.77.174301.

Kohlhauser, C., and C. Hellmich, 2012, Determination of Poisson's ratios in isotropic, transversely isotropic, and orthotropic materials by means of combined ultrasonic-mechanical testing of normal stiffnesses: Applications to metals and wood: European Journal of Mechanics A/Solids, **33**, 82–98, doi: 10.1016/j.euromechsol.2011.11.009.

Li, X., 2006, On approximate analytic expressions for the velocity of Rayleigh waves: Wave Motion, **44**, 120–127, doi: 10.1016/j.wavemoti.2006.07.003.

Martinez, J., and D. Schmitt, 2013, Anisotropic elastic moduli of carbonates and evaporites from the Weyburn-Midale reservoir and seal rocks: Geophysical Prospecting, **61**, 363–379, doi: 10.1111/1365-2478.12032.

Mavko, G., T. Mukerji, and J. Dvorkin, 1998, The rock physics handbook: Tools for seismic analysis in porous media: Cambridge University Press.

Mechkour, H., 2002, The exact expressions for the roots of Rayleigh wave equation: *in* V. Balan, ed., Proceedings of the International Colloquium of Mathematics in Engineering and Numerical Physics (MENP2), vol. 8, Geometry Balkan Press, 96–104.

Möllhoff, M., C. J. Bean, and P. G. Meredith, 2010, Rock fracture compliance derived from time delays of elastic waves: Geophysical Prospecting, **58**, 1111–1121, doi: 10.1111/j.1365-2478.2010.00887.x.

Musgrave, M. J. P., 1970, Crystal acoustics: Holden-Day.

Najafi, S., V. Bucur, and G. Ebrahimi, 2005, Elastic constants of particleboard with ultrasonic technique: Materials Letters, **59**, 2039–2042, doi: 10.1016/j.matlet.2005.02.013.

Nkemzi, D., 2008, A simple and explicit algebraic expression for the Rayleigh wave velocity: Mechanics Research Communications, **35**, 201–205, doi: 10.1016/j.mechrescom.2007.10.005.

Nolte, D. D., L. J. Pyrak-Nolte, J. Beachy, and C. Ziegler, 2000, Transition from the displacement discontinuity limit to the resonant scattering regime for fracture interface waves: International Journal of Rock Mechanics and Mining Sciences, **37**, 219–230, doi: 10.1016/S1365-1609(99)00102-1.

Pyrak-Nolte, L. J., and D. D. Nolte, 1995, Wavelet analysis of velocity dispersion of elastic interface waves propagating along a fracture: Geophysical Research Letters, **22**, 1329–1332, doi: 10.1029/95GL01323.

Rahman, M., and J. Barber, 1995, Exact expressions for the roots of the secular equation for Rayleigh waves: Journal of Applied Mechanics, **62**, no. 1, 250–252, doi: 10.1115/1.2895917.

Rahman, M., and T. Michelitsch, 2006, A note on the formula for the Rayleigh wave speed: Wave Motion, **43**, 272–276, doi: 10.1016/j.wavemoti.2005.10.002.

Rayleigh, L., 1885, On waves propagated along the plane surface of an elastic solid: Proceedings of the Royal Society of London, **17**, 4–11, doi: 10.1112/plms/s1-17.1.4.

Sanders, P., and D. Yuhas, 2007, Frictional material elastic property round robin study: Presented at 25th Annual Brake Colloquium.

Schoenberg, M., and C. Sayers, 1995, Seismic anisotropy of fractured rock: Geophysics, **60**, 204–211, doi: 10.1190/1.1443748.

Shao, S., and L. J. Pyrak-Nolte, 2013, Interface waves along fractures in anisotropic media: Geophysics, **78**, no. 4, T99–T112, doi: 10.1190/geo2012-0464.1.

Sharf-Aldin, M., R. Rosen, S. Narasimhan, and M. PaiAngle, 2013, Experience using a novel 45 degree transducer to develop a general unconventional Shale geomechanical model: Presented at 47th Annual American Rock Mechanics Association Conference, 1–20.
Taylor, J. R., 1997, An introduction to error analysis: The study of uncertainties in physical measurements: University Science Books.
Thomsen, L., 1986, Weak elastic anisotropy: Geophysics, **51**, 1954–1966, doi: 10.1190/1.1442051.
Tsvankin, I., 1996, P-wave signatures and notation for transversely isotropic media: An overview: Geophysics, **61**, 467–483, doi: 10.1190/1.1443974.
Tsvankin, I., 1997, Anisotropic parameters and P-wave velocity for orthorhombic media: Geophysics, **62**, 1292–1309, doi: 10.1190/1.1444231.
Vestrum, R., 1994, Group and phase velocity inversions for the general anisotropic stiffness tensor: M.S. thesis, University of Calgary.
Vinh, P., and R. W. Ogden, 2004a, Formulas for the Rayleigh wave speed in orthotropic elastic solids: Archives of Mechanics, **56**, 247–265.
Vinh, P., and R. W. Ogden, 2004b, On formulas for the Rayleigh wave speed: Wave Motion, **39**, 191–197, doi: 10.1016/j.wavemoti.2003.08.004.
Wang, L., 1995, Determination of the ray surface and recovery of elastic constants of anisotropic elastic media: A direct and inverse approach: Journal of Physics: Condensed Matter, **7**, 3863–3880, doi: 10.1088/0953-8984/7/20/007.
Wolfe, J., 1998, Imaging phonons: Acoustic wave propagation in solids: Cambridge University Press.